NANO LETTERS

2009
Vol. 9, No. 8
2978-2983

Integrating a High-Force Optical Trap with Gold Nanoposts and a Robust Gold−DNA Bond

D. Hern Paik,[†] Yeonee Seol,[†,§] Wayne A. Halsey,[†] and Thomas T. Perkins*[,†,‡]

JILA, National Institute of Standards and Technology and University of Colorado, Boulder, Colorado 80309, and Department of Molecular, Cellular, and Developmental Biology, University of Colorado, Boulder, Colorado 80309

Received May 2, 2009

ABSTRACT

Gold-thiol chemistry is widely used in nanotechnology but has not been exploited in optical-trapping experiments due to laser-induced ablation of gold. We circumvented this problem by using an array of gold nanoposts ($r = 50-250$ nm, $h \approx 20$ nm) that allowed for quantitative optical-trapping assays without direct irradiation of the gold. DNA was covalently attached to the gold via dithiol phosphoramidite (DTPA). By using three DTPAs, the gold−DNA bond was not cleaved in the presence of excess thiolated compounds. This chemical robustness allowed us to reduce nonspecific sticking by passivating the unreacted gold with methoxy-(polyethylene glycol)-thiol. We routinely achieved single beads anchored to the nanoposts by single DNA molecules. We measured DNA's elasticity and its overstretching transition, demonstrating moderate- and high-force optical-trapping assays using gold-thiol chemistry. Force spectroscopy measurements were consistent with the rupture of the strepavidin−biotin bond between the bead and the DNA. This implied that the DNA remained anchored to the surface due to the strong gold−thiol bond. Consistent with this conclusion, we repeatedly reattached the trapped bead to the same individual DNA molecule. Thus, surface conjugation of biomolecules onto an array of gold nanostructures by chemically and mechanically robust bonds provides a unique way to carry out spatially controlled, repeatable measurements of single molecules.

Optical trapping's broad force range (0.01−100's pN) coupled with its atomic-scale (0.1 nm) sensitivity enables a multitude of studies,[1−3] including stretching DNA,[4] characterizing molecular motors,[5] unfolding proteins,[6] and rupturing protein−ligand bonds.[7] These assays require coupling biomolecules to surfaces through mechanically strong bonds. Often the challenging part in such assays is maintaining biological activity while minimizing nonspecific sticking.[3] Ideally, one would like to pattern biomolecules on an otherwise nonstick surface. Gold-thiol chemistry can provide an important, complementary conjugation technique to the commonly used, but mechanically weaker, ligand−receptor couplings (e.g., streptavidin−biotin, digoxigenin−antidigoxigenin). Gold-thiol bonds are covalent and therefore mechanically strong (∼1.4 nN).[8] Gold is also easy to pattern at the nanometer scale.[9] However, gold-thiol chemistry is not used in optical-trapping applications due to laser-induced ablation of the gold.

Nanopatterning offers a means to optimize the spacing between individual molecules. Usually, the surface distribution of molecules in these assays is random and is controlled by varying the concentration and duration of a binding step. Yet, different single-molecule assays require different spacing between molecules. For example, consider an optical-trapping assay using DNA (Figure 1a). If the DNA molecules are too close together, then two beads (anchored by separate DNA molecules) can fall into the same trap, or two DNA molecules can bind to one bead. At low surface densities, bead-DNA complexes are widely spaced and time-consuming to find. In either limit, data collection is inefficient. Thus, controlled spacing of single molecules can enhance the efficiency and throughput of these assays.

This optimization needs to maintain biological activity, which is hindered by the ubiquitous problem of nonspecific sticking. Uncontrolled surface adsorption can lead to reduction (or loss) of activity. Further, such molecules can sterically interfere with studies of nearby molecules. Nonspecific sticking is most effectively reduced by coating glass coverslips with polyethylene-glycol (PEG).[10] However, this PEGylation is a multistep, labor intensive process. Moreover, the resulting spatial distribution of molecules is still random and can vary from day to day.

* To whom correspondence should be addressed. E-mail: tperkins@jila.colorado.edu.
[†] JILA, National Institute of Standards and Technology and University of Colorado.
[‡] Department of Molecular, Cellular, and Developmental Biology, University of Colorado.
[§] Current address: Laboratory of Molecular Biophysics, NHLBI, National Institutes of Health, Bethesda, Maryland 20892.

10.1021/nl901404s CCC: $40.75
Published on Web 06/03/2009

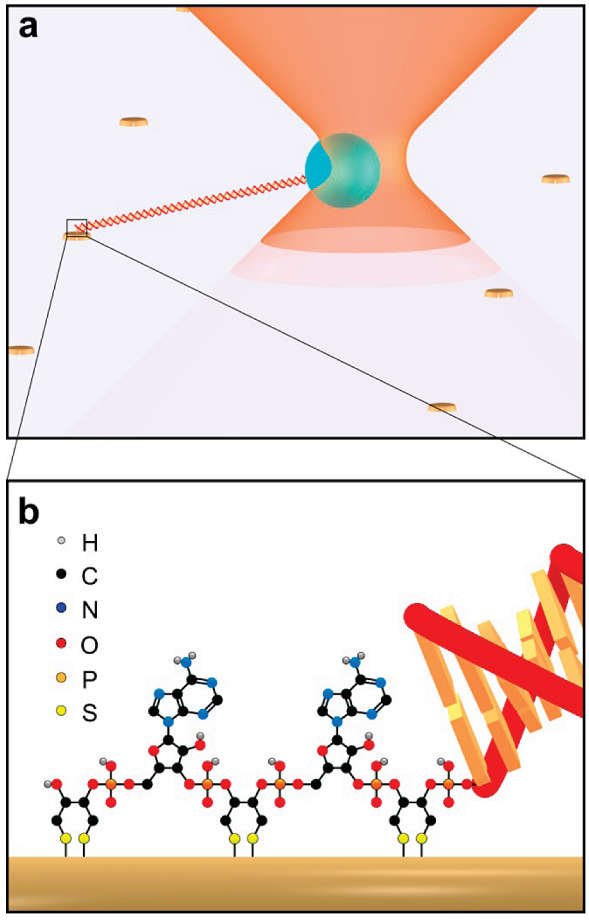

Figure 1. (a) Schematic of an optical-trapping assay integrated with an array of gold nanoposts (not to scale). The DNA was anchored at one end via a gold-DTPA bond while the opposite end was attached to an optically trapped streptavidin-coated bead via biotin. The posts were on an $8 \times 8\ \mu m^2$ grid with a lateral offset of 4 μm between adjacent rows. (b) Chemical structure of DTPA linker attached to gold surface, where adenine bases were placed between the repeated DTPA moiety to provide flexibility and spacing for higher binding efficiency. Hydrogens on carbon atoms are not shown.

Maintaining biological activity often requires a reducing agent [e.g., 1 mM dithiothreitol (DTT)]. While mechanically strong, single gold−thiol bonds are not stable in the presence of such high levels of thiolated compounds. Multiple gold−thiol bonds lead to more chemically robust attachment.[11,12] Specifically, DNA anchored by three repetitions of dithiol phosphoramidite (DTPA, Glen Research) is not displaced by millimolar concentrations of hexanethiol.[13] DTPA-labeled oligonucleotides are commercially available and can be used as primers for polymerase chain reaction. Thus, DTPA provides a robust and accessible means to anchor DNA to gold.[13,14]

Gold-thiol conjugation is used in single-molecule atomic force microscopy (AFM)[15] and, more recently, magnetic-tweezers studies.[16] In this letter, we report the successful integration of optical traps with gold-supported bioconjugation at site specific locations. Specifically, we developed a set of experimental procedures for quantitative optical-trapping assays that avoided the direct irradiation of an array of gold nanoposts ($r_{post} = 50-250$ nm, $h_{post} \approx 20$ nm). With multivalent attachment [3 DTPAs (Figure 1b)], the DNA remained bound in the presence of 10 mM thiolated compounds (DTT and β-mercaptoethanol). This chemical robustness allowed us to significantly lower nonspecific sticking by coupling methoxy-(polyethylene glycol)-thiol (mPEG-SH) to the unreacted gold. We attached the opposite end of the DNA to streptavidin-coated beads using a 5′-biotin label. With this assay, we measured DNA's elasticity, its overstretching transition, and the biotin−streptavidin bond's rupture force. By holding the detached bead near the nanopost with minimal laser power (~250 μW), we reattached the bead to the surface-anchored DNA. The mean change in anchor location before and after reattachment was ~5 nm, indicating that the same individual DNA molecule was repeatedly measured (see below).

By using a spatially defined array of nanoposts, we targeted the DNA to specific locations that were visible in an optical microscope using standard (Köhler) illumination. We optimized the distribution of posts by considering (i) the DNA contour length [$L = 2081$ nm (6230 base pairs)] and bead radius ($r_{bd} = 345$ nm); (ii) the 70% increase in DNA extension during the force-induced overstretching of the DNA at 65 pN;[4,17] and (iii) the geometric area needed to determine the DNA's anchor point via elasticity measurements along the coordinate axes. Our optimized geometry has posts on a $8 \times 8\ \mu m^2$ grid with a 4 μm offset between adjacent rows (Figure 1a; Supporting Information, Figure S1). We fabricated this array of nanoposts on KOH-cleaned glass coverslips using physical vapor deposition of gold through silicon-nitride-membrane shadow masks (Figure 2a).[18] Deposition at a base pressure of $\leq 8 \times 10^{-7}$ Torr (0.1 mPa) led to good coupling of the DNA to the gold. To prevent clogging of the shadow mask, we cleaned the masks after each use by alternating soaking in aqua regia (3:1 volume ratio of HNO_3/HCl) (*Hazard*) and a nitric-acid based chromium etchant (TFN, Transene, Inc.) (*Hazard*). We reused individual shadow masks multiple times ($N > 50$). Use of shadow masks avoided exposing the unreacted gold to the chemical solution normally used to remove a polymeric mask.

To further maintain the reactivity of the gold, we incubated the DTPA-labeled DNA immediately after deposition. The number of DNA molecules per nanopost depended on the DNA concentration, incubation time, and post size. Using flow cells formed from patterned coverslips, we optimized the assay to achieve beads anchored by single DNA molecules (at the expense of fractional occupancy). Our protocol consisted of sequentially adding the DNA, passivating the gold with methoxy-(polyethylene glycol)-thiol (mPEG-SH, MW = 5 kD, Nektar), passivating the glass with bovine serum albumin (BSA), and finally attaching the streptavidin beads to the DNA (Figure 2b−e; Supporting Information). Under conditions that promoted anchoring by single molecules, visual inspection showed a 10% fractional occupancy (~25 tethers per 221 posts). At higher DNA concentration, a fractional occupancy of 50% was achieved, though with 50% of the beads anchored by multiple DNAs.

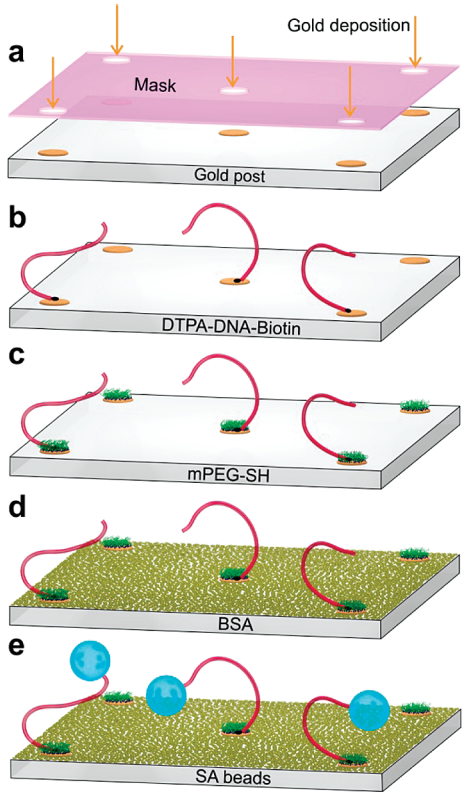

Figure 2. Steps for making gold nanoposts and attaching bead-DNA complexes to them (not to scale). (a) Gold was deposited onto a glass coverslip through a Si_3N_4 membrane shadow mask (purple). (b) DNA (red), end-labeled with DTPA (black dot), was incubated with freshly deposited gold. (c) The unreacted gold was passivated with mPEG-SH (green). (d) The cover glass was passivated with bovine serum albumin (BSA) (olive). (e) Streptavidin-coated beads were attached to biotinylated end of the DNA.

Control experiments demonstrated that mPEG-SH-coated surfaces exhibited excellent nonstick properties for single-molecule experiments. We tested this using coverslips coated with a thin, continuous layer of gold and passivated with mPEG-SH. Such coverslips showed dramatically reduced nonspecific sticking of protein-coated beads (~10 stuck beads per 1 × 1 mm^2) even without added blocking agents (BSA and Tween-20, a nonionic detergent used to reduce sticking). For comparison, this is 20-fold better than glass coverslips coated with BSA and using a solution containing both BSA (3 mg/mL) and Tween-20 (0.4%).

Our optical-trapping microscope used two lasers, one at high power (400 mW at focus) and a second at much lower power (250 μW). The first laser beam formed the optical trap. The second, weaker beam measured bead position using back-focal-plane detection.[19] Except for calibration of detector sensitivity, we left the trap stationary and colinear with the detection laser. We moved the sample in three dimensions (3D) via a closed-loop, piezoelectric (PZT) stage. Details of the trap were similar to prior reports.[20−22] Calibrations followed the standard protocols[23] and yielded a trap stiffness of 1 pN/nm using 400 mW and a 345-nm radius bead.

The first step in a single-molecule optical-trapping experiment is to verify that a single molecule is being studied and to establish the proper trapping geometry. For DNA, single-molecule anchoring is demonstrated by measuring DNA's elasticity[24] and fitting the resulting data to a wormlike chain model (WLC).[25] If the fit returns a persistence length, p, (a measure of polymer stiffness) of ~50 nm,[26] then a single DNA molecule is being studied. To measure DNA's elasticity, the location of the DNA's attachment to the cover glass, often called its tether point, must be aligned to the trap in 3D. The tether point's vertical position is found by monitoring the change in forward-scattered light as a trapped bead is brought into contact with the surface by raising the stage.[27] Next, an elasticity-centering procedure symmetrically stretches the DNA along positive and negative directions on the x- and y-axes. For each axis, this routine returns three values, p, L, and Δ, where L is the DNA contour length and Δ is the offset of the tether point relative to the optical-trapping axis. A first iteration of this procedure roughly locates the anchor point of the DNA, and a second iteration refines this location and quantitatively measures p and L.

Punctate anchoring of DNA to gold was integrated with modified optical-trapping procedures to avoid direct laser irradiation of the gold (Figure 3). With both trap and detection lasers off, we visually centered a nanopost containing a tethered bead under the stationary trap (Figure 3a). Next, we laterally moved the nanopost ~1 μm along the x-axis and turned on both lasers, which led to rapid trapping of the tethered bead (Figure 3b). At this position, we scanned the stage vertically until the trapped bead was in contact with the glass surface and moved the surface 300 nm below the contact point (not shown). We then measured the elasticity of the DNA along both the negative and positive y directions (Figure 3c−d) and fitted the resulting data to the WLC model to determine p, L, and Δ (Figure 4a). We used p and L to select for beads anchored by single DNA molecules. Both lasers were turned off, and we corrected for the y-lateral offset (Δ) by a stage movement (Figure 3e). The process was then repeated along the x-axis (Figure 3f−j). We repeated steps a−j two more times to determine the anchor point more accurately. Convergence in anchor point location was excellent; Δ for the third iteration was a mere 1.7 ± 3.7 and 0.1 ± 2.2 nm (mean ± std. dev.; $N = 28$) in the x- and y-axes, respectively.

Quantitative interpretation of these elasticity curves required a modification to the standard method for determining DNA elasticity in a surface-coupled assay.[23] Our elasticity curves were taken at a substantial lateral offset (~1 μm) to the direction of stretching to avoid ablation of the gold. We recorded bead displacement, and hence force, along the axis of stage motion. The 3D force-extension curve was calculated from this 1D projection by an extension of earlier work[23] using both a lateral and a vertical offset (see Supporting Information; Figures S2, S3). With this correction, we reproduced the expected persistence length ($p = 44.6$ nm for this length DNA)[21] [e.g., Figure 4a, $p = 49$ nm; see also Figure 5b inset, $\langle p \rangle = 42.1 \pm 0.3$ nm (mean ± std. err.; $N = 196$)]. Summarizing, we performed a quantitative optical-

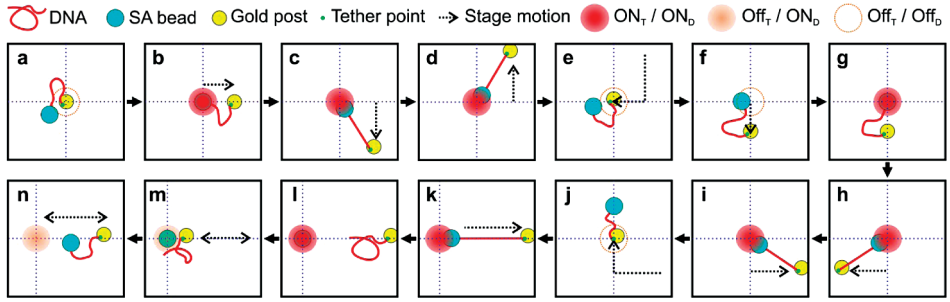

Figure 3. Procedure for measuring DNA anchored to a gold nanopost with an optical trap (not to scale). The trap and the colinear detection lasers were stationary during the experiment (intersection of the dotted lines), while the sample was moved in 3D via a PZT stage. The on/off states of trap and detection lasers are indicated by shading. A 2D elasticity-centering routine (a−j) determined the anchor point of the DNA along the *y*- and *x*-axes sequentially, similar to prior work[27] but with a substantial (∼1 μm) lateral offset. Steps a−j were repeated two more times to localize the anchor point with nanometer-scale precision. By moving the stage at constant velocity (k), high forces were exerted on the DNA that ultimately resulted in the rupture of the biotin-streptavidin bond anchoring the DNA to the bead (l). To reattach the bead to the same individual DNA molecule, the disconnected bead was trapped by a weak detection beam, positioned near the post, and then slowly moved back and forth (m) until the bead rebound to the DNA and the stage motion pulled the bead out of the weak trap (n).

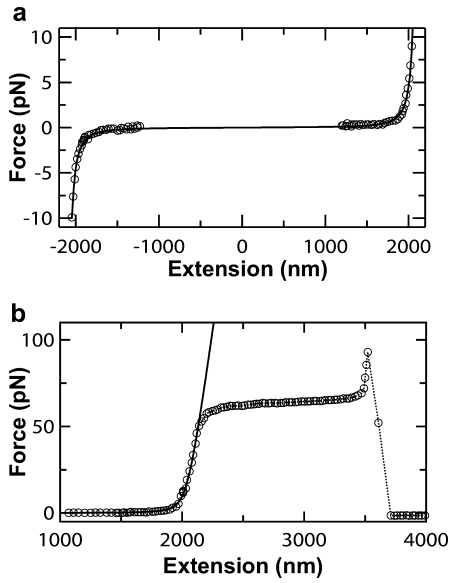

Figure 4. Force-extension records of DNA molecules at moderate and high forces. (a) Elasticity measurement of the 2081 nm (6230 base pairs) long DNA tether (circle) stretched up to 10 pN in the positive and negative directions. Using a fitting routine that takes into account the substantial lateral offset (∼1 μm) relative to the DNA length (Supporting Information), we fit the data to the WLC model[25] (line) to determine three values, p, L, and Δ, where p is the persistence length, L is the contour length, and Δ is the location of the anchor point. For the trace shown, the fitted values were 48.9 (±1.6) nm, 2093 (±2) nm, and 0.2 (±0.5) nm, respectively. Data between −1200 and 1200 nm were not used in the fitting process, and the determined p was insensitive to this exclusion.[21] (b) Force-extension record for DNA when moving the stage at a uniform velocity (250 nm/s) (circles). The plateau at ∼65 pN corresponds to the overstretching transition of the DNA. The cusp at 90 pN corresponds to the rupture of the biotin−streptavidin bond. The force-extension record below 50 pN is well fit by a WLC model that includes enthalpic stretching of the DNA backbone (line).[31]

trapping experiment at moderate forces (<10 pN) while using a gold−thiol bond to anchor a biological molecule.

We next demonstrated integration of gold−thiol bonds in assays that required higher forces (>100 pN) and therefore higher laser powers (400 mW). Numerous single-molecule assays require high forces, including bacteriophage portal proteins (55 pN),[28] overstretching DNA (65 pN),[4,17] and rupture of ligand−receptor bonds (≤200 pN depending on loading rate).[29,30]

In the overstretching transition, DNA undergoes a remarkable structural transition at ∼65 pN in which its extension increases to 1.7 times its contour length over a small force range (ΔF = 5 pN).[4,17] To measure this transition, we laterally offset the anchor point from the trap center by ∼1 μm and then turned on the trap to a high power. After the bead was captured (not shown), we moved the stage at a constant velocity (250 nm/s) in the same direction as the offset until the tether failed (Figure 3k,l; Figure 4b). The plateau at ∼65 pN corresponds to the overstretching transition. We interpret the cusp at 90 pN as a failure in the linkage between the bead and the surface followed by the bead returning to the center of the trap (F = 0 pN).

The characteristic shape and force of the overstretch transition provided a complementary way to distinguish single tethers from multiple tethers. First, below 50 pN, the force-versus-extension data were well modeled by a WLC model of a single DNA molecule that incorporated an enthalpic stretch modulus[31] (1200 pN/nm) (Figure 4b, black line). Second, multiply tethered beads, identified by low p, also showed multiple cusps along with abnormal overstretching and rupture curves. For example, in tethers that we interpreted as multiple tethers (p < 25 nm), we found more than one cusp in the overstretching experiment (Supporting Information, Figure S4). And, finally, the characteristic force ($F_{\text{overstretch}}$) of the transition was 64.9 ± 0.5 pN (mean ± std. err; N = 58), in agreement with prior reports.[4,17] Thus, this qualitative and quantitative agreement with prior overstretching results demonstrates high-force optical-trapping while using DNA anchored to gold.

We hypothesized that the rupture in the DNA tether was due to the failure of the streptavidin−biotin bond, since the covalent gold−thiol bond anchoring the DNA to the surface should be significantly stronger. If true, then the DNA

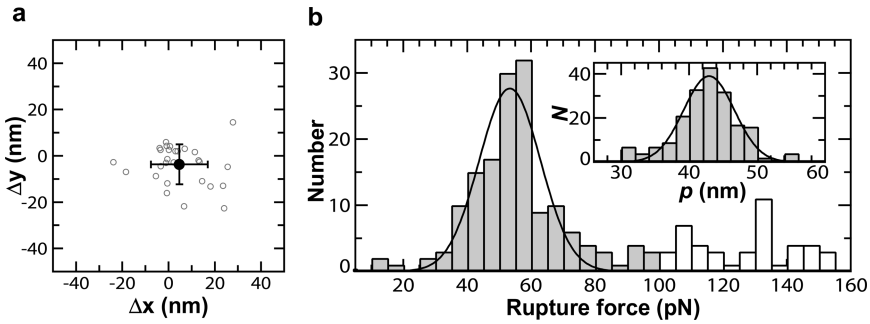

Figure 5. (a) Distribution of the difference between tether points (Δx, Δy) before and after a rupture of the bead-DNA linkage and subsequent rebinding via fishing [4.7 ± 12.3 and -3.7 ± 8.6 nm (mean $\pm$ std. dev.; $N = 28$), for x and y respectively]. (b) Histogram of biotin−streptavidin rupture forces obtained at a stage velocity of 250 nm/s ($N = 196$). The most probable rupture force [53.3 ± 0.9 pN ($N = 153$)] deduced by fitting the peak (gray shading) to a Gaussian (black). Inset: histogram of p for the molecules studied in panel b.

remained attached to the surface at the location previously determined via the DNA elasticity-centering routines. We attempted to reattach the trapped bead to the DNA in a "fishing" process similar to the in situ construction of bead-DNA-bead complexes used in combined micropipette optical-trapping assays.[32]

To confine the bead near the prior anchor point without significantly heating the gold, we held the bead slightly offset (∼20−50 nm) from the edge of the gold nanoposts using the weak detection laser (250 μW). We intermittently moved the sample ∼1 μm laterally to probe for reattachment (Figure 3m). When the bead reattached (∼2 min), the bead pulled out of the weak trap formed by the detection laser (Figure 3n). After successful reattachment, we repeated the 2D elasticity-centering protocol previously discussed to determine the anchor point (Figure 3a−j).

The anchor point locations before and after rebinding were essentially identical, indicating that the same individual DNA molecule was remeasured. If the bead had attached to a different DNA molecule randomly distributed over the gold nanopost, we would expect a lateral offset in both x and y comparable to the radius of the nanopost ($r_{post} = 50-250$ nm). In contrast to this large offset, we measured a lateral offset of 4.7 ± 12.3 and -3.7 ± 8.6 nm (mean $\pm$ std. dev.) in x and y, respectively, for 28 rebindings using 14 different molecules (Figure 5a). This precise localization shows reattachment of the bead to the same individual DNA molecule. Additionally, we observed that beads initially anchored by multiple DNAs rebound to multiple DNAs whereas beads anchored by single DNAs rebound to single DNAs. These results suggest that beads anchored by single DNA molecules result from a nanopost containing only a single DNA.

The streptavidin−biotin bond has a characteristic rupture force ($F_{rupture}$) that depends on the loading rate ($\partial F/\partial t$). Single-molecule force-spectroscopy should yield this characteristic $F_{rupture}$. By using a moderate loading rate (∼100 pN/s), we biased $F_{rupture}$ to a lower value amenable to optical trapping. Since we used DNA, our experiment had three distinct loading rates (100, 1, and 200 pN/s) around 65 pN (Figure 4b). Notwithstanding this complication, the most probable $F_{rupture}$, based on a Gaussian fit to the peak shown in Figure 5b, was 53.3 ± 0.9 pN, which is in agreement with prior results ($F_{rupture} \approx 57$ pN at 100 pN/s),[30] but with a broader distribution. A fraction of the tethers (22%) survived over 100 pN. While the origin of these high $F_{rupture}$ is unknown, rupture events of >100 pN were not due to multiple tethers. These tethers had both the correct p and $F_{overstretch}$ (Supporting Information, Figure S5). Overall, these force spectroscopy results demonstrate that the streptavidin−biotin bond was the weak link in our assay and emphasize the strength of the gold−thiol bond relative to the strongest noncovalent biological interactions.

Looking forward, we foresee several enhancements to the techniques developed here. (i) Smaller posts (<50 nm) provide a means for a higher fraction of posts to be labeled with single molecules, since steric/electrostatic repulsion due to the binding of the first DNA molecule should reduce the probability of a second one binding. (ii) Rebinding to (or "fishing" for) surface-anchored DNA could be significantly accelerated by stretching the DNA laterally with either an electric field[33] or a fluid flow,[34] causing the end of the DNA to overlap the trapped bead and thereby promote binding.[32] (iii) Enzymes that bind to or move along DNA can be coupled to beads[35] and positioned near the DNA, allowing for rapid in situ assembly of a single-DNA, single-protein assay (polymerases,[36] helicases,[37] etc.,). Finally, (iv) Multi-thiolated mPEG could be used to create excellent nonstick surfaces compatible with DTT.

A multitude of important single-molecule experiments use DNA longer than 1 μm.[24,28,38,39] Nonetheless, the most stringent limitation in the current generation of this assay is the requirement for a moderately long tether between the surface-anchor point and the optical trap that eliminates the laser-induced ablation of the gold. This modest (1 μm) spatial separation arises from the tightly focused ($w_0 = 427$ nm)[20] trap. Smaller posts and lower laser powers may help alleviate this geometric constraint.

In conclusion, we successfully integrated gold-thiol chemistry into single-molecule optical-trapping experiments at both moderate and high forces. More generally, we expect that anchoring DNA by the mechanically and chemically robust DTPA bond will be useful in other single-molecule assays ranging from AFM to fluorescence studies. The chemical robustness enables specific anchoring of biomolecules to gold concurrent with the reduction of nonspecific

sticking to gold by mPEG-SH. The mechanical strength assures that the DNA remains bound to the same surface location, so the same individual molecule can be repeatedly probed by either an optical trap or an AFM. Indeed, the site-specific anchoring via patterned nanostructures (e.g., DNA molecule on nanopost at row 12, column 9) enables measuring the same individual molecule across different force measurement platforms (optical trap and AFM), a goal in the development of picoNewton-scale force standards based on intrinsic molecular properties. Thus, we expect this chemistry, complementary to existing digoxigenin and biotin conjugation but mechanically much stronger, to be broadly useful in single-molecule biophysics, picoscale force standards, and potentially the controlled assembly of DNA-based nanostructures.

Acknowledgment. This work was supported by a National Research Council Research Associateship (D.H.P.), a W. M. Keck Grant in the RNA Sciences, the National Science Foundation (Phy-0404286), and NIST. Mention of commercial products is for information only; it does not imply NIST's recommendation or endorsement. T.T.P. is a staff member of NIST's Quantum Physics Division.

Supporting Information Available: Detailed descriptions of shadow-mask preparation and deposition of gold, DNA preparation, tethered-bead assay, and analysis of DNA force-extension records with both lateral and vertical offsets. Figures show optimizing nanoposts spacing for studying the DNA overstretch transition (Figure S1), geometry of stretching DNA with lateral and vertical offsets (Figure S2), force-extension curves with and without lateral-offset correction (Figure S3), force-extension curves for beads anchored by multiple DNAs (Figure S4), and a scatter plot of persistence length and overstretching force for DNA tethers with $F_{\text{rupture}} > 100$ pN (Figure S5). This material is available free of charge via the Internet at http://pubs.acs.org.

References

(1) Neuman, K. C.; Block, S. M. *Rev. Sci. Instrum.* **2004**, *75*, 2787–2809.
(2) Moffitt, J. R.; Chemla, Y. R.; Smith, S. B.; Bustamante, C. *Annu. Rev. Biochem.* **2008**, *77*, 205–228.
(3) Perkins, T. T. *Laser Photonics Rev.* **2009**, *3*, 203–220.
(4) Smith, S. B.; Cui, Y.; Bustamante, C. *Science* **1996**, *271*, 795–799.
(5) Svoboda, K.; Schmidt, C. F.; Schnapp, B. J.; Block, S. M. *Nature* **1993**, *365*, 721–727.
(6) Cecconi, C.; Shank, E. A.; Bustamante, C.; Marqusee, S. *Science* **2005**, *309*, 2057–2060.
(7) Zhang, Y.; Sun, G.; Lu, S.; Li, N.; Long, M. *Biophys. J.* **2008**, *95*, 5439–5448.
(8) Grandbois, M.; Beyer, M.; Rief, M.; Clausen-Schaumann, H.; Gaub, H. E. *Science* **1999**, *283*, 1727–1730.
(9) Zhao, X. M.; Xia, Y. N.; Whitesides, G. M. *J. Mater. Chem.* **1997**, *7*, 1069–1074.
(10) Ha, T.; Rasnik, I.; Cheng, W.; Babcock, H. P.; Gauss, G. H.; Lohman, T. M.; Chu, S. *Nature* **2002**, *419*, 638–641.
(11) Dougan, J. A.; Karlsson, C.; Smith, W. E.; Graham, D. *Nucleic Acids Res.* **2007**, *35*, 3668–3675.
(12) Li, Z.; Jin, R. C.; Mirkin, C. A.; Letsinger, R. L. *Nucleic Acids Res.* **2002**, *30*, 1558–1562.
(13) Liepold, P.; Kratzmueller, T.; Persike, N.; Bandilla, M.; Hinz, M.; Wieder, H.; Hillebrandt, H.; Ferrer, E.; Hartwich, G. *Anal. Bioanal. Chem.* **2008**, *391*, 1759–1772.
(14) Rosi, N. L.; Giljohann, D. A.; Thaxton, C. S.; Lytton-Jean, A. K. R.; Han, M. S.; Mirkin, C. A. *Science* **2006**, *312*, 1027–1030.
(15) Krautbauer, R.; Rief, M.; Gaub, H. E. *Nano Lett.* **2003**, *3*, 493–496.
(16) Walter, N.; Selhuber, C.; Kessler, H.; Spatz, J. P. *Nano Lett.* **2006**, *6*, 398–402.
(17) Cluzel, P.; Lebrun, A.; Heller, C.; Lavery, R.; Viovy, J. L.; Chatenay, D.; Caron, F. *Science* **1996**, *271*, 792–794.
(18) Carter, A. R.; King, G. M.; Perkins, T. T. *Opt. Express* **2007**, *15*, 13434–13445.
(19) Visscher, K.; Gross, S. P.; Block, S. M. *IEEE J. Sel. Top. Quantum Electron.* **1996**, *2*, 1066–1076.
(20) Seol, Y.; Carpenter, A. E.; Perkins, T. T. *Opt. Lett.* **2006**, *31*, 2429–2431.
(21) Seol, Y.; Li, J.; Nelson, P. C.; Perkins, T. T.; Betterton, M. D. *Biophys. J.* **2007**, *93*, 4360–4373.
(22) Carter, A. R.; Seol, Y.; Perkins, T. T. *Biophys. J.* **2009**, *96*, 2926–2934.
(23) Wang, M. D.; Yin, H.; Landick, R.; Gelles, J.; Block, S. M. *Biophys. J.* **1997**, *72*, 1335–1346.
(24) Smith, S. B.; Finzi, L.; Bustamante, C. *Science* **1992**, *258*, 1122–1126.
(25) Marko, J. F.; Siggia, E. D. *Macromolecules* **1995**, *28*, 8759–8770.
(26) Hagerman, P. J. *Annu. Rev. Biophys. Biophys. Chem.* **1988**, *17*, 265–286.
(27) Perkins, T. T.; Dalal, R. V.; Mitsis, P. G.; Block, S. M. *Science* **2003**, *301*, 1914–1918.
(28) Smith, D. E.; Tans, S. J.; Smith, S. B.; Grimes, S.; Anderson, D. L.; Bustamante, C. *Nature* **2001**, *413*, 748–752.
(29) Florin, E.-L.; Moy, V. T.; Gaub, H. E. *Science* **1994**, *264*, 415–417.
(30) Merkel, R.; Nassoy, P.; Leung, A.; Ritchie, K.; Evans, E. *Nature* **1999**, *397*, 50–53.
(31) Odijk, T. *Macromolecules* **1995**, *28*, 7016–7018.
(32) Wuite, G. J. L.; Davenport, R. J.; Rappaport, A.; Bustamante, C. *Biophys. J.* **2000**, *79*, 1155–1167.
(33) Smith, S. B.; Aldridge, P. K.; Callis, J. B. *Science* **1989**, *243*, 203–206.
(34) Perkins, T. T.; Smith, D. E.; Larson, R. G.; Chu, S. *Science* **1995**, *268*, 83–87.
(35) Neuman, K. C.; Abbondanzieri, E. A.; Landick, R.; Gelles, J.; Block, S. M. *Cell* **2003**, *115*, 437–447.
(36) Wang, M. D.; Schnitzer, M. J.; Yin, H.; Landick, R.; Gelles, J.; Block, S. M. *Science* **1998**, *282*, 902–907.
(37) Perkins, T. T.; Li, H. W.; Dalal, R. V.; Gelles, J.; Block, S. M. *Biophys. J.* **2004**, *86*, 1640–1648.
(38) Wuite, G. J.; Smith, S. B.; Young, M.; Keller, D.; Bustamante, C. *Nature* **2000**, *404*, 103–106.
(39) Bustamante, C.; Bryant, Z.; Smith, S. B. *Nature* **2003**, *421*, 423–427.

NL901404S